

OPEN ACCESS

Highly Dense Mn-Co Spinel Coating for Protection of Metallic Interconnect of Solid Oxide Fuel Cells

To cite this article: Sung-Il Lee *et al* 2014 *J. Electrochem. Soc.* **161** F1389

View the [article online](#) for updates and enhancements.

You may also like

- [White light emitting diodes with super-high luminous efficacy](#)
Yukio Narukawa, Masatsugu Ichikawa, Daisuke Sanga *et al.*
- [In_{0.49}GaP/Al_{0.49}GaAs Barrier Enhancement-Mode Pseudomorphic High Electron Mobility Transistor with High Gate Turn-on Voltage and High Linearity](#)
Kyoungchul Jang, Juyong Lee, Jaehak Lee *et al.*
- [Lithium-Sulfur Batteries with an Ultrahigh-Sulfur-Loading Carbon-Cotton Cathode](#)
Sheng-Heng Chung, Chi-Hao Chang and Arumugam Manthiram



Your Lab in a Box!

The PAT-Tester-i-16: All you need for Battery Material Testing.

- ✓ All-in-One Solution with integrated Temperature Chamber!
- ✓ Cableless Connection for Battery Test Cells!
- ✓ Fully featured Multichannel Potentiostat / Galvanostat / EIS!

www.el-cell.com +49 40 79012-734 sales@el-cell.com

EL-CELL[®]
electrochemical test equipment





Highly Dense Mn-Co Spinel Coating for Protection of Metallic Interconnect of Solid Oxide Fuel Cells

Sung-II Lee, Jongsup Hong, Hyoungchul Kim, Ji-Won Son,* Jong-Ho Lee, Byung-Kook Kim, Hae-Weon Lee, and Kyung Joong Yoon^z

High-Temperature Energy Materials Research Center, Korea Institute of Science and Technology, Seoul, South Korea

The major degradation issues of solid oxide fuel cells (SOFC) are associated with the oxide scale growth and Cr evaporation of the metallic interconnect. To address these challenges, a highly dense spinel oxide coating was fabricated on a ferritic stainless steel interconnect using a cost-competitive ceramic processing route. The nano-scale $\text{Mn}_{1.5}\text{Co}_{1.5}\text{O}_4$ spinel powder was synthesized using a glycine-nitrate method, and the particle agglomerates were effectively disintegrated by a high-energy attrition milling process. The spinel protective coating, which was applied by screen printing, was sintered to a nearly full density, without causing damage to the metallic substrate, by a high-temperature annealing process in a reducing environment, followed by re-oxidation at a moderate temperature. The dense spinel coating remarkably reduced the growth rate of chromia scale and restrained the evaporation of chromium species, as verified by area specific resistance (ASR) measurements and analysis on chromium distribution over the cross-section. Strong adhesion between the coating and substrate was confirmed after 500-hour operation. The sintering mechanism involved in reduction-oxidation heat-treatment was studied based on dilatometry measurements and microstructural features. The implication of the ASR change and the chromium migration for stability of practical SOFC stacks was discussed in detail.

© The Author(s) 2014. Published by ECS. This is an open access article distributed under the terms of the Creative Commons Attribution 4.0 License (CC BY, <http://creativecommons.org/licenses/by/4.0/>), which permits unrestricted reuse of the work in any medium, provided the original work is properly cited. [DOI: 10.1149/2.0541414jes] All rights reserved.

Manuscript submitted August 12, 2014; revised manuscript received September 30, 2014. Published October 8, 2014.

Solid oxide fuel cells (SOFCs) represent one of the most environmentally friendly and versatile technologies for generation of electrical power and heat from a variety of fuels through electrochemical reactions.¹⁻³ Because a single cell produces less than 1 V under typical SOFC operating conditions, SOFC stacks are configured using multiple cells to obtain the desired voltage and power output for practical power generation. In SOFC stacks, the primary functions of the interconnect are to connect the anode of one cell to the cathode of the next one electrically and to separate the fuel from the oxidant in adjoining cells. At the initial stage of SOFC development, acceptor-doped lanthanum chromite had been the most popular ceramic interconnect material for the high-temperature stacks that operate at approximately 1000°C.⁴⁻⁷ In recent years, progress in anode-supported planar design technology with thin electrolytes led to the reduction of operating temperatures below 800°C, which enabled the use of high-temperature oxidation-resistant alloys as alternatives.^{4,8,9} These metallic interconnect materials offer many advantages over their ceramic counterparts, such as high electric and thermal conductivities, low cost, ease of manufacturing and good workability.¹⁰ Among various candidate materials, chromia-forming ferritic alloys are considered to be promising because the chromia scale on the surface exhibits relatively high electrical conductivity and low growth rate.¹¹ However, most of the commercially available ferritic alloys impose degradation issues associated with continuous oxide scale growth and evaporation of chromium species under the SOFC operating conditions. Currently, it is extremely difficult to satisfy the general stability criteria for stationary SOFC stacks, such as a degradation rate of 0.25%/kh and a service life of five years,^{12,13} when using commercial high-temperature oxidation-resistant alloys as interconnect materials.

The main degradation issues of metallic interconnect in SOFC stacks include the increase of area specific resistance (ASR) resulting from continuous oxide scale growth, surface instability because of oxidation/spallation, and chromium poisoning of the cathode caused by evaporation of chromium-containing species from the interconnect.^{9,14-16} To overcome the inherent weaknesses of the chromia-forming ferritic alloys upon exposure to high temperatures, significant research efforts have been devoted to developing the protective coating techniques.^{9,17,18} The key requirements for a protective coating include dense structure, high electronic conductivity, thermal, mechanical and chemical compatibility with the adjacent components and low diffusion coefficients of Cr and O. Among coating mate-

rials, such as reactive element oxides,^{11,19-24} nitrides,²⁵⁻²⁷ conductive perovskites²⁸⁻³⁹ and conductive spinels,^{10,35,40-49} $\text{Mn}_{1.5}\text{Co}_{1.5}\text{O}_4$ spinel has been actively investigated by many researchers for its excellent electrical conductivity, thermal expansion match with ferritic alloys and chromium retention capability.^{41,42,50-55} For fabrication of dense and well-adherent protective spinel coating layers, various deposition techniques have been investigated, including screen printing,^{50,56,57} dip coating,^{47,58-60} electroplating,^{53,61-63} plasma spray,^{64,65} thermal spray,⁶⁶ electrophoretic deposition,^{10,49,67} physical vapor deposition,^{68,69} aerosol deposition,⁷⁰ sol-gel^{46,71} and pack cementation.^{72,73} Although the feasibility of these techniques has been substantiated, individual processes exhibit their characteristic drawbacks along with their advantages. For example, electroplating is suitable for uniformly applying thin film over a complex configuration, but the large negative reduction potential of manganese makes the control of the spinel composition extremely difficult.¹⁸ The vacuum deposition processes could provide high-quality thin films but may be inadequate for mass production because of high costs and low deposition rate.¹⁸ Considering manufacturing costs, processing simplicity and scalability, slurry coating techniques such as screen printing could be attractive choices, but the subsequent high-temperature sintering step for removal of open pores readily leads to abnormal oxide scale growth and interfacial defect formation. Although advanced processing techniques, such as field-assisted sintering,⁷⁴ reaction sintering⁶⁰ and flash-sintering,⁷⁵ have been proposed to lower the sintering temperature of the spinel layer, densifying the oxide coating layer without damaging the metallic substrate remains challenging. Therefore, it is highly desirable to develop the fabrication techniques for a dense and well-adherent protective coating layer on a metallic interconnect based on a cost-effective slurry coating for commercial development and deployment of SOFC technologies.

In this study, nano-scale $\text{Mn}_{1.5}\text{Co}_{1.5}\text{O}_4$ spinel powder was synthesized using a glycine-nitrate process, and a completely dense coating with strong adhesion to the metallic interconnect was fabricated based on a screen printing technique. This study modified the heat-treatment processing conditions to avoid damage to the substrate. The protection capability of the spinel coating against oxidation scale growth and evaporation of chromium-containing species was investigated by ASR measurements and structural / compositional analysis.

Experimental

The $\text{Mn}_{1.5}\text{Co}_{1.5}\text{O}_4$ spinel powder was synthesized using the glycine nitrate process.³⁹ The precursors of manganese and cobalt nitrates

*Electrochemical Society Active Member.

^zE-mail: kjyoon@kist.re.kr

were mixed in distilled water according to the desired stoichiometric ratio, and glycine was added as a combustion fuel. The concentration of the solution was 0.8 M and the glycine-to-nitrate ratio was 0.55. Combustion was performed on a hot plate, and the resulting powders were calcined at 800°C for 2 hours in air. The crystal structure and phase purity of the powder were analyzed using X-ray diffraction (XRD). The calcined powder was attrition-milled in ethanol with the desired amount of dispersant for 2 hours, and the change of particle morphology by attrition milling was examined using scanning electron microscopy (SEM), transmission electron microscopy (TEM) and Brunauer-Emmett-Teller (BET) analysis. The cylindrical specimens were prepared by uniaxially pressing the powder at 100 MPa, and sintering shrinkages were measured using a dilatometer in air and 4% H₂-96% N₂ up to 1000°C.

The Mn_{1.5}Co_{1.5}O₄ spinel paste was prepared by mixing the powders with the desired amounts of solvent, dispersant, binder and plasticizer using a planetary mill. A commercial ferritic stainless steel, Crofer 22 APU, with the composition of 22.8 wt% Cr, 0.45 wt% Mn, 0.08 wt% Ti, 0.06 wt% La, Al 0.0056 wt% Al, 0.10 wt% Si, 0.0046 wt% Cu, 0.0009 wt% Ce, 0.005 wt% C and the balance in Fe, was used as the substrate for the coating. The substrates were prepared by cutting a Crofer 22 APU block into rectangular pieces with the dimension of 5 mm × 5 mm × 8 mm. These pieces were polished with SiC sandpapers up to 1200 grits and ultrasonically cleaned in acetone and ethanol for 10 minutes each. The paste was screen-printed on both sides of the Crofer 22 APU substrate and heat-treated in air and 4% H₂-96% N₂ between 800 and 1000°C. The gas atmosphere was switched at high temperature. The effect of the sintering conditions on the microstructure of the coating layer was investigated by examining the surface and cross-section of the spinel coating using SEM. The ASR's of the bare and coated samples were measured at 800°C in dry air for 500 hours using a four probe DC technique. The bare samples were pre-oxidized at 800°C in air for 100 hours. For current collection, the sample was placed between two Pt meshes (5 mm×5 mm) and pressed using the spring load. Each Pt mesh was connected to two Pt wires. One was used to apply the current, and the other to measure the voltage. A constant current density of 100 mA cm⁻² was applied to the sample for ASR measurements. After testing, the microstructure and elemental distribution were examined using SEM and energy dispersive X-ray spectroscopy (EDS) analysis, respectively.

Results and Discussion

Figure 1 shows the XRD patterns of the Mn-Co spinel (Mn_{1.5}Co_{1.5}O₄) powder synthesized by the glycine-nitrate process. The XRD pattern reveals the formation of a dual phase mixture of

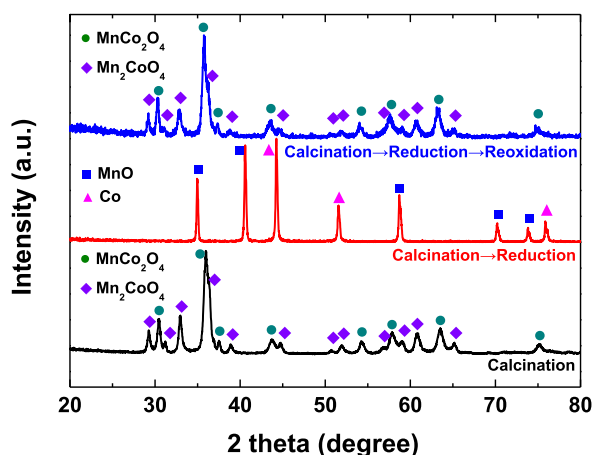


Figure 1. XRD patterns of Mn_{1.5}Co_{1.5}O₄ powders after calcination at 800°C in air, after reduction at 800°C in humidified forming gas (3% H₂O+3% H₂+94% N₂) and after re-oxidation at 800°C in air.

MnCo₂O₄ and Mn₂CoO₄ after calcination at 800°C in air. No characteristic peaks of secondary or impurity phases were observed. The MnCo₂O₄ is a normal cubic spinel with Mn on octahedral interstitial sites and with Co on both tetrahedral and octahedral interstitial sites in the face-centered cubic configuration of the oxygen ion lattice.⁷⁶ The Mn₂CoO₄ is an intermediate tetragonal spinel phase between the cubic MnCo₂O₄ and tetragonal Mn₃O₄ (Mn²⁺[Mn³⁺]₂O₄).⁷⁷ The tetragonal distortion of (Mn,Co)₃O₄ spinel occurs when the content of Mn³⁺ ions exceeds the critical value, approximately 60%.⁷⁸ Based on the thermodynamic study of Mn_{1+δ}Co_{2-δ}O₄ spinel, the cubic and tetragonal phases co-exist for 0.3 < δ < 0.9, whereas a single phase cubic spinel is stable for δ < 0.3 and a single phase tetragonal spinel is stable for δ > 0.9,⁷⁹ which is consistent with the observations in this study. The high-temperature XRD analysis showed that the dual phase spinel transforms into a single phase material at high temperatures. The nominal composition of Mn_{1.5}Co_{1.5}O₄ is considered to be the most promising Mn-Co spinel formulation as a protective coating material for SOFC metallic interconnect because of its excellent electrical conductivity and its thermal expansion match with the Crofer 22 APU interconnect.^{51,77} The conductivity of Mn_{1.5}Co_{1.5}O₄ is ~60 S cm⁻¹ at 800°C in air,³⁵ and the thermal expansion coefficients of Mn_{1.5}Co_{1.5}O₄ and Crofer 22 APU are 11.4×10⁻⁶ K⁻¹ and 12.6×10⁻⁶ K⁻¹, respectively.⁷⁷ In the fabrication of the spinel protective coating layer, the intermediate heat-treatment in a reducing atmosphere could effectively enhance the film density and adhesion to the ferritic stainless steel substrate.^{42,51} Upon exposure to a reducing atmosphere (4% H₂-96% N₂) at 800°C, the Mn-Co spinel is reduced to MnO and metallic Co as confirmed by XRD analysis in Figure 1. This implies that the Mn-Co spinel is not stable in the anode environment and the application of the spinel as a protection layer for the metallic interconnect is limited to the cathode side. In a subsequent re-oxidation heat-treatment in air at 800°C, the MnO and Co reform the original spinel phase (Figure 1) via the following reactions:⁷⁷



The morphology of Mn_{1.5}Co_{1.5}O₄ powder synthesized by the glycine-nitrate process is presented in Figure 2. The glycine-nitrate process is a self-sustaining combustion technique for synthesizing nano-scale ceramic powders from an aqueous solution of metal nitrate and glycine.⁸⁰ This technique provides excellent powder characteristics such as controlled particle size and compositional homogeneity if the precursor stoichiometric ratio and reaction conditions are carefully adjusted.^{18,81} The TEM image of the powder calcined at 800°C (Figure 2a) shows extremely fine particles with uniform size distribution. The size of the primary particles is 30~50 nm. In general, the sintering temperature of the nano-crystalline powder is significantly lower than that of regular powder because of the large surface area and the high surface energy.⁸²⁻⁸⁴ However, the sintering behavior of the nano-crystalline powder could be disturbed by the presence of

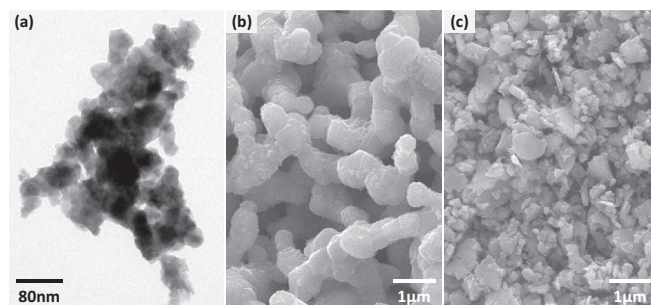


Figure 2. (a) TEM and (b) SEM images of the Mn_{1.5}Co_{1.5}O₄ powder calcined at 800°C in air, and (c) SEM image of the powder after attrition milling for 2 hours.

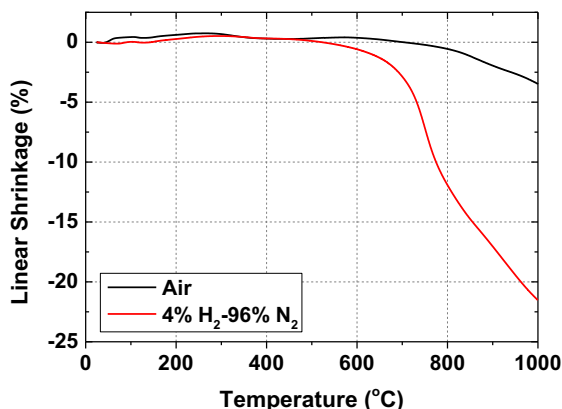


Figure 3. Linear sintering shrinkage of $\text{Mn}_{1.5}\text{Co}_{1.5}\text{O}_4$ spinel measured by dilatometer between 25 and 1000°C in oxidizing (air) and reducing (4% H_2 -96% N_2) atmospheres.

particle agglomerates.⁸⁵ The low-magnification SEM image of the calcined powder in Figure 2b reveals the substantial amount of agglomerates formed by partial sintering of the nano-crystallites during synthesis and subsequent calcination. The mean particle size is 0.8 μm , which is larger than the primary particles by more than an order of magnitude. To reduce the degree of agglomeration, high-energy attrition milling was performed on the calcined powder. The SEM image of the attrition-milled powder in Figure 2c shows that the hard agglomerates were effectively broken down. The effect of attrition milling was also confirmed by BET analysis that showed an increase in the specific surface area from 3.50 $\text{m}^2 \text{g}^{-1}$ to 22.34 $\text{m}^2 \text{g}^{-1}$. Therefore, it is suggested that the glycine-nitrate technique, followed by an optimal milling process, is a promising method for synthesizing nano-crystalline spinel powder with a homogeneous morphology.

Figure 3 shows the linear sintering shrinkage of the $\text{Mn}_{1.5}\text{Co}_{1.5}\text{O}_4$ powder compacts in oxidizing and reducing environments as a function of temperature. In air, sintering begins at approximately 700°C, and less than 2% of sintering shrinkage is observed at 800°C. In general, it is favorable to densify the green coating of the Mn-Co spinel at a low temperature, preferably below 800°C, because the high-temperature process causes excessive growth of the oxide scale on the surface of the metallic interconnect, leading to an increase in the electrical resistance and fatal damage to the structural integrity.^{60,86} In particular, it was reported that exposing Crofer 22 APU to the temperatures higher than 800°C in an oxidizing atmosphere accelerates the attacks associated with the formation of hematite nodules on the surface of the scale, causing severe metal loss.¹⁵ However, it is well-known that Mn-Co spinel is extremely difficult to densify at such a low temperature in air,⁶⁰ as confirmed by dilatometry measurements in Figure 3. On the contrary, in a reducing atmosphere (4% H_2 -96% N_2), the onset temperature of sintering is substantially lower (below 600°C), and the linear shrinkage at 800°C is 12% (Figure 3). This suggests that the sinterability of the mixture of MnO and Co is significantly higher than that of the Mn-Co spinel. In addition, because the growth of the oxide scale on the surface of the ferritic alloy is suppressed in the reducing environment,¹⁵ the green coating could possibly be processed above 800°C without causing severe damage to the metallic interconnect. At 1000°C, sintering shrinkage reaches 21%, suggesting that nearly complete densification of the protective coating could be achieved. The shrinkage in reducing atmosphere could be influenced by both sintering and decomposition of spinel. As confirmed by XRD analysis in Figure 1, spinel completely decomposes into MnO and Co at 800°C. Therefore, the shrinkage observed above 800°C should be dominated by sintering of MnO and Co, rather than decomposition of spinel structure. Subsequently, the original spinel structure could be restored by the re-oxidation process at moderate processing temperatures, as shown by the XRD analysis in Figure 1.

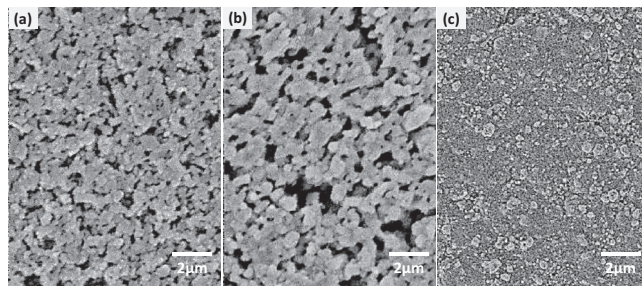


Figure 4. SEM images of the surface of a $\text{Mn}_{1.5}\text{Co}_{1.5}\text{O}_4$ spinel coating; (a) annealed in air at 800°C, (b) reduced in 4% H_2 -96% N_2 and re-oxidized in air at 800°C and (c) reduced in 4% H_2 -96% N_2 at 1000°C followed by reoxidation in air at 800°C.

The $\text{Mn}_{1.5}\text{Co}_{1.5}\text{O}_4$ spinel coatings were applied to Crofer 22 APU substrates by screen-printing, and the surface morphology was examined by SEM after the various heat-treatments, as shown in Figure 4. The SEM image of the sample sintered at 800°C in air (Figure 4a) shows a highly porous structure with small grains. In Figure 4b, the spinel layer was heat-treated in a reducing atmosphere (4% H_2 -96% N_2) at 800°C for 24 hours, followed by re-oxidation in air at 800°C for 24 hours. Grain growth caused by the reduction-oxidation cycle is clearly observed. The average grain size increased from $\sim 0.5 \mu\text{m}$ in Figure 4a to $\sim 1.1 \mu\text{m}$ in Figure 4b. Although local densification appears to be enhanced by the addition of the reduction step at 800°C, large pores remaining in the coating layer would still allow the transport of gaseous species during high-temperature operations. However, the protective spinel coating, which was reduced at 1000°C and subsequently re-oxidized at 800°C, shows a very dense surface, free of visible pores and cracks in Figure 4c. Therefore, it is suggested that the enhanced sintering activity of the composite of MnO and Co enables the coating to reach a sufficiently high density at 1000°C in a reducing atmosphere as predicted by the dilatometry measurements (Figure 3). The study also suggests that porosity could be further reduced by incorporating elemental oxygen during re-oxidation at 800°C.⁸⁷ Moreover, a reaction-sintering mechanism could enhance densification during the re-oxidation process because the enthalpy of reaction to form the Mn-Co spinel from MnO and Co (equation 1 and 2) provides an additional driving force for sintering beyond the reduction of the surface energy,^{48,54} leading to the very dense protective coating in Figure 4c.

The cross-sectional SEM images of the $\text{Mn}_{1.5}\text{Co}_{1.5}\text{O}_4$ spinel coating layers after various heat-treatments are displayed in Figure 5. The thickness of the coating was uniform at 4~5 μm , and the coating was well-adhered to the substrate without any indication of cracking or delamination. Figure 5 clearly exhibits the effects of the processing parameters on the final density and microstructure of the coating. The $\text{Mn}_{1.5}\text{Co}_{1.5}\text{O}_4$ spinel coating layer sintered at 800°C in air in Figure 5a contains a large number of open pores, and the particle size is very small. After reduction in 4% H_2 -96% N_2 and re-oxidation in air at 800°C, the density of the coating layer significantly increases, and grain growth is observed in Figure 5b. However, large through-pores are locally observed, which suggests that the protective coating could not completely block the migration of chromium and oxygen species. Figure 5c shows that the reduction process at the elevated temperature (1000°C) followed by re-oxidation at 800°C could successfully form a completely dense coating without causing excessive growth of the oxide scale or any structural damage to the metallic substrate. The oxide scale of Crofer 22 APU is composed of a chromia inner layer and a $(\text{Mn,Cr})_3\text{O}_4$ spinel outer layer, which is formed by the diffusion of Mn along the grain boundaries of the chromia scale.⁸⁸ The boundary between the Mn-Co spinel protection layer and the Mn-Cr spinel intrinsic scale on Crofer 22 APU is not clearly observed, which suggests that the coating layer and the substrate are chemically and thermo-mechanically compatible, forming the strong interface.

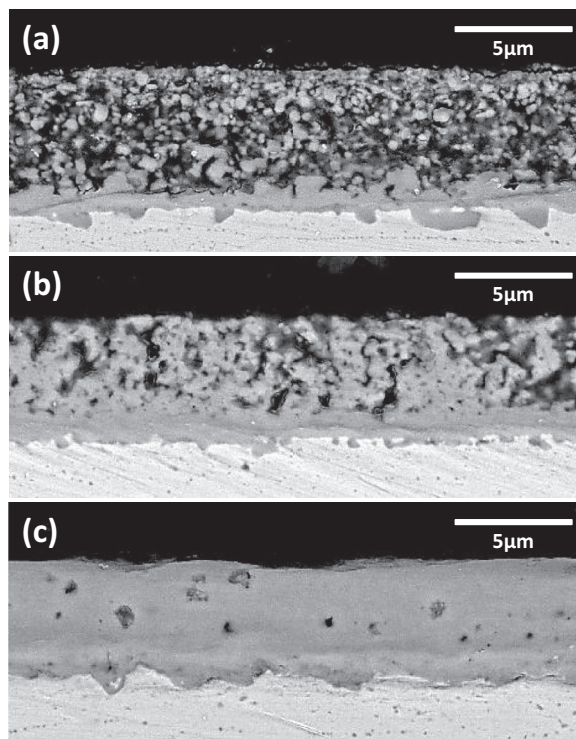


Figure 5. SEM images of the cross-section of a $\text{Mn}_{1.5}\text{Co}_{1.5}\text{O}_4$ spinel coating; (a) after annealing in air at 800°C , (b) after reduction in 4% H_2 -96% N_2 and re-oxidation in air at 800°C and (c) after reduction in 4% H_2 -96% N_2 at 1000°C followed by reoxidation in air at 800°C .

Figure 6 compares the ASR data of the bare and coated Crofer 22 APU samples measured at 800°C in air for 500 hours. The ASR value was obtained using the following equation:^{89,90}

$$\text{ASR} = \frac{1}{2} \times \frac{V}{I} A \quad [3]$$

where V is the voltage drop across the sample, I is the applied current, and A is the area. The factor $1/2$ in equation 3 is used because the measured resistance is contributed by the oxide scale formed on both sides of the sample. The thickness of the samples used for ASR measurements was 8 mm, and measurement results were divided by two for ASR calculations (equation 3). Therefore, the ASR data presented in Figure 6 should be close to the ASR of the practical interconnect

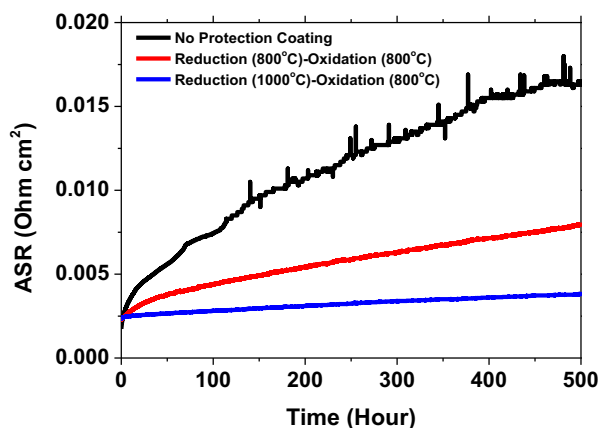


Figure 6. ASR data of the uncoated Crofer 22 APU sample, the sample with coating reduced and re-oxidized at 800°C , and the sample with coating reduced at 1000°C and re-oxidized at 800°C , measured at 800°C in air for 500 hours.

in SOFC stacks, whose thickness is generally 2~4 mm for a planar design.^{91,92} The electrical resistance of the metallic interconnect with a protective coating includes the contributions of the bulk metal, the oxide scale and the coating layer. In general, the bulk resistance of oxidation-resistant alloys such as Crofer 22 APU is extremely low, and the electrical behavior is dominated by the resistance of the scale and the coating.⁹³ In Figure 6, the initial ASR of the uncoated Crofer 22 APU was slightly lower than those of coated samples because there was no additional resistance from the spinel coating layer. However, the ASR of the uncoated sample increased rapidly upon exposure to high temperature and overtook those of coated samples within 10 hours of operation. The ASR value of the uncoated sample was initially 0.0016 Ohm cm^2 and reached 0.017 Ohm cm^2 after 500 hours. During the SOFC operation, growth of the chromia inner scale on Crofer 22 APU, whose thickness could reach several micrometers on the cathode side, is mainly responsible for the increase of ohmic ASR of the stack,⁹ and the rapid increase of ASR in the uncoated sample in Figure 6 corresponds to the fast degradation of stack performance. In addition, the formation of interfacial defects, such as voids, cavities and spallation, is also an important factor that influences the stability of the SOFC stacks.^{94,95} The scattering of the ASR data is observed for the uncoated sample after ~ 120 hours of operation, which could be ascribed to the structural instability at the interface.⁹⁶ It was reported that the interfacial strength between the metallic interconnect and the oxide scale decreases with the growth of the chromia scale, and the thick scale readily causes spallation because of the increased thermal stress.^{40,97} Therefore, the ASR data of the uncoated sample in Figure 6 emphasizes the importance of the protective coating to block the inward migration of oxygen for interfacial stability. The ASR data of the coated samples in Figure 6 clearly show that protective coatings effectively suppress the growth of the chromia scale. Two types of protective coatings were evaluated in this experiment: One of them was reduced and re-oxidized at 800°C , and the other was reduced at 1000°C and re-oxidized at 800°C . As shown in Figure 5, the former contains residual porosity, referred to as a “porous coating,” whereas the latter is completely dense and labeled a “dense coating.” The starting ASR of the sample with the porous coating was 0.0023 Ohm cm^2 , which was close to that of the sample with the dense coating. However, the ASR value for the sample with the porous coating increased at a substantially higher rate during operations, and reached 0.0081 Ohm cm^2 after 500 hours while the ASR value for the sample with the dense coating was 0.0037 Ohm cm^2 after the same duration of time under the same conditions. In general, the metallic SOFC interconnects with the state-of-the-art protective coating show the ASR values of 5~10 mOhm cm^2 after 500~1000 hours of operation,^{9,18} and the ASR results in Figure 6 indicate that the spinel coating presented in this paper is promising. The spikes of the ASR values, which occurred in the uncoated sample after ~ 120 hours of operation, were not observed for both samples up to 500 hours, indicating that the interfaces remained stable and free of structural damage. The ASR curves of all of the samples show a parabolic growth tendency because the oxide scale growth is governed by the diffusion-controlled kinetics.⁹⁰ Based on extrapolating 500 hours of the ASR data (Figure 6) and assuming parabolic growth, the ASR value is predicted to be 0.015 Ohm cm^2 at the target service life of five years^{8,17} for the Crofer 22 APU with a dense coating, which is significantly lower than the conventional ASR goal of 0.1 Ohm cm^2 for a SOFC interconnect.^{4,9} Therefore, it is suggested that the use of a dense $\text{Mn}_{1.5}\text{Co}_{1.5}\text{O}_4$ protective coating, which is formed by reduction at the elevated temperature ($\sim 1000^\circ\text{C}$) followed by re-oxidation at moderate temperature ($\sim 800^\circ\text{C}$), effectively impedes the oxidation kinetics and enhances the structural stability of the ferritic alloys, which may satisfy the durability targets for stationary SOFC applications.

In addition to blocking the inward migration of oxygen, the protection layer should serve as a barrier to the outward transport of chromium-containing species. The chromium in the ferritic interconnect readily reacts with oxygen and forms vapor phases, which then migrate into the cathode and deposit on the electrochemically active sites, resulting in electrode poisoning and

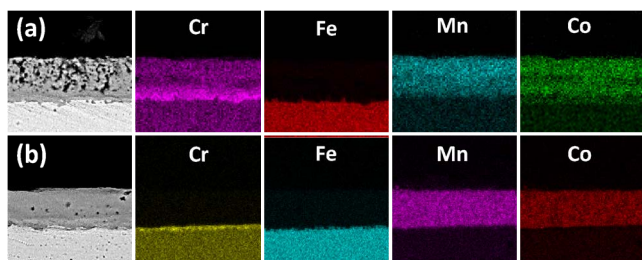
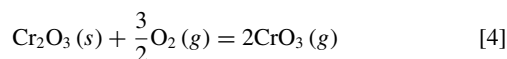


Figure 7. SEM images and EDS analysis of the coated samples used for ASR measurements at 800°C for 500 hours: (a) reduction and re-oxidation at 800°C and (b) reduction at 1000°C followed by re-oxidation at 800°C.

performance degradation.^{98,99} Chromium in the 6+ oxidation state, which is highly volatile, is the major gaseous species, and the vaporization of chromium in dry air could be described as;⁹⁶



One of the most obvious indications of the outward migration of the chromium-containing species is the presence of chromium inside and on the surface of the pores of the protection layer. The EDS analysis of the cross-sections of the samples used for ASR measurements at 800°C for 500 hours indicates that no detectable chromium penetrated the dense $\text{Mn}_{1.5}\text{Co}_{1.5}\text{O}_4$ spinel coating layer formed by reduction at 1000°C followed by re-oxidation at 800°C (Figure 7a). On the contrary, a substantial amount of chromium was detected in the porous protection layer, which was fabricated by reduction and re-oxidation at 800°C (Figure 7b). The concentration of Cr was 0.72 wt% inside the coating and 0.65 wt% outer interface based on the quantitative EDS analysis. Therefore, the results shown in Figure 7 indicate the importance of the film density for the chromium retention capability of the protective coating. In addition, it is reconfirmed that the dense spinel protective coating effectively prevents the inward migration of oxygen because the Cr-rich subscale beneath the dense coating was substantially thinner ($\sim 0.5 \mu\text{m}$) than that beneath the porous coating ($1.5 \mu\text{m}$), as clearly seen in the Cr maps in Figure 7. The formation of interfacial defects, which could contribute to the increase of ASR, was not observed after 500-hours of operation.

Based on the results presented in this paper, the dense $\text{Mn}_{1.5}\text{Co}_{1.5}\text{O}_4$ spinel protective coating effectively suppresses the migration of oxygen and chromium-containing species, resulting in improved electrical and structural stability. The reducing heat-treatment is an important intermediate process for densifying the protective coating layer and could be performed at sufficiently high temperatures without causing fatal damage to the metallic substrate. The properties of the spinel coating are expected to be further enhanced by optimizing the composition and processing parameters.

Conclusions

One of the most severe sources of degradation in SOFC stacks is associated with the metallic interconnect, and a protective coating layer is necessary to address the durability issues related to the growth of oxide scale and the evaporation of chromium. In this study, the dense $\text{Mn}_{1.5}\text{Co}_{1.5}\text{O}_4$ spinel protective coating was successfully fabricated by optimizing the powder synthesis, coating and heat-treatment techniques. In particular, the intermediate reduction process at the elevated temperature remarkably improved the density of the coating layer without damaging the metallic substrate. The dense protective coating effectively reduced the growth rate of the oxide scale and the evaporation of chromium-containing species. In this paper, the coating was applied by screen printing, which can only be used on flat or nearly flat surfaces, while the practical SOFC interconnects are complex-shaped with grooves and tilted surfaces. Therefore, our forthcoming paper will focus on developing the processing technique

to uniformly cover the practical SOFC interconnect with the dense protective coating and evaluating the stability of the metallic interconnect in the SOFC stack configuration.

Acknowledgments

This research was financially supported by the institutional research program of the Korea Institute of Science and Technology and the Fusion Research Program for Green Technologies through the National Research Foundation of Korea (NRF) and funded by the Ministry of Education, Science and Technology (NRF-2011-0019297).

References

1. N. Q. Minh, *Journal of the American Ceramic Society*, **76**, 563 (1993).
2. S. C. Singhal, *Solid State Ionics*, **135**, 305 (2000).
3. S. C. Singhal, *Solid State Ionics*, **152**, 405 (2002).
4. W. Z. Zhu and S. C. Deevi, *Materials Science and Engineering: A*, **348**, 227 (2003).
5. T. R. Armstrong, J. S. Hardy, S. P. Simner, and J. W. Stevenson, in, p. 706. *Solid Oxide Fuel Cells (SOFC VI). Proceedings of the Sixth International Symposium*, Pennington, NJ, USA (1999).
6. N. Sakai, H. Yokokawa, T. Horita, and K. Yamaji, *International Journal of Applied Ceramic Technology*, **1**, 23 (2004).
7. S. P. S. Badwal and K. Foger, *Ceramics International*, **22**, 257 (1996).
8. W. Z. Zhu and S. C. Deevi, *Materials Research Bulletin*, **38**, 957 (2003).
9. J. Wu and X. Liu, *Journal of Materials Science & Technology*, **26**, 293 (2010).
10. H. Abdoli and P. Alizadeh, *Materials Letters*, **80**, 53 (2012).
11. K. Huang, P. Y. Hou, and J. B. Goodenough, *Materials Research Bulletin*, **36**, 81 (2001).
12. W. A. Surdoyal and I. Lee, *DOE's SECA and FutureGen Programs: Progress and Plans*, p. 1296, Ieee, New York (2008).
13. W. A. Surdoyal, in *Solid Oxide Fuel Cells 10*, K. Eguchi, S. C. Singhal, H. Yokokawa, and H. Mizusaki Editors, p. 11, Electrochemical Society Inc, Pennington (2007).
14. Z. Yang, G.-G. Xia, M. S. Walker, C.-M. Wang, J. W. Stevenson, and P. Singh, *International Journal of Hydrogen Energy*, **32**, 3770 (2007).
15. Z. Yang, M. S. Walker, P. Singh, J. W. Stevenson, and T. Norby, *Journal of The Electrochemical Society*, **151**, B669 (2004).
16. S. Megel, E. Girdauskaite, V. Sauchuk, M. Kusnezoff, and A. Michaelis, *Journal of Power Sources*, **196**, 7136 (2011).
17. M. Bertoldi, D. Montinaro, A. Fossati, A. Lavacchi, C. Giolli, V. M. Sglavo, T. Zandonella, and U. Bardi, *Journal of Fuel Cell Science and Technology*, **5**, 011001 (2008).
18. N. Shaigan, W. Qu, D. G. Ivey, and W. Chen, *Journal of Power Sources*, **195**, 1529 (2010).
19. W. Qu, L. Jian, D. G. Ivey, and J. M. Hill, *Journal of Power Sources*, **157**, 335 (2006).
20. S. Fontana, R. Amendola, S. Chevalier, P. Piccardo, G. Caboche, M. Viviani, R. Molins, and M. Sennou, *Journal of Power Sources*, **171**, 652 (2007).
21. W. Qu, J. Lia, and D. G. Ivey, *Journal of Power Sources*, **138**, 162 (2004).
22. D. E. Alman and P. D. Jablonski, *International Journal of Hydrogen Energy*, **32**, 3743 (2007).
23. N. Oishi, T. Namikawa, and Y. Yamazaki, *Surface and Coatings Technology*, **132**, 58 (2000).
24. J. S. Yoon, J. Lee, H. J. Hwang, C. M. Whang, J.-W. Moon, and D.-H. Kim, *Journal of Power Sources*, **181**, 281 (2008).
25. A. Kayani, R. J. Smith, S. Teintze, M. Kopezyk, P. E. Gannon, M. C. Deibert, V. I. Gorokhovskoy, and V. Shutthanandan, *Surface and Coatings Technology*, **201**, 1685 (2006).
26. X. Liu, C. Johnson, C. Li, J. Xu, and C. Cross, *International Journal of Hydrogen Energy*, **33**, 189 (2008).
27. J. Wu, C. Li, C. Johnson, and X. Liu, *Journal of Power Sources*, **175**, 833 (2008).
28. C. Johnson, R. Gemmen, and N. Orlovskaya, *Composites Part B: Engineering*, **35**, 167 (2004).
29. N. Orlovskaya, A. Coratolo, C. Johnson, and R. Gemmen, *Journal of the American Ceramic Society*, **87**, 1981 (2004).
30. I. Belogolovsky, X.-D. Zhou, H. Kurokawa, P. Y. Hou, S. Visco, and H. U. Anderson, *Journal of The Electrochemical Society*, **154**, B976 (2007).
31. J. H. Zhu, Y. Zhang, A. Basu, Z. G. Lu, M. Paranthaman, D. F. Lee, and E. A. Payzant, *Surface and Coatings Technology*, **177-178**, 65 (2004).
32. K. Hilpert, D. Das, M. Miller, D. H. Peck, and R. Weiß, *Journal of The Electrochemical Society*, **143**, 3642 (1996).
33. Y.-J. Yang, T.-L. Wen, H. Tu, D.-Q. Wang, and J. Yang, *Solid State Ionics*, **135**, 475 (2000).
34. Z. Yang, G.-G. Xia, G. D. Maupin, and J. W. Stevenson, *Journal of The Electrochemical Society*, **153**, A1852 (2006).
35. Z. Yang, G.-G. Xia, G. D. Maupin, and J. W. Stevenson, *Surface and Coatings Technology*, **201**, 4476 (2006).
36. Y. Larring and T. Norby, *Journal of The Electrochemical Society*, **147**, 3251 (2000).
37. J.-J. Choi, J.-H. Lee, D.-S. Park, B.-D. Hahn, W.-H. Yoon, and H.-T. Lin, *Journal of the American Ceramic Society*, **90**, 1926 (2007).
38. J.-J. Choi, D.-S. Park, B.-D. Hahn, J. Ryu, and W.-H. Yoon, *Journal of the American Ceramic Society*, **91**, 2601 (2008).

39. C.-L. Chu, J.-Y. Wang, and S. Lee, *International Journal of Hydrogen Energy*, **33**, 2536 (2008).
40. X. Chen, P. Y. Hou, C. P. Jacobson, S. J. Visco, and L. C. De Jonghe, *Solid State Ionics*, **176**, 425 (2005).
41. C. C. Mardare, H. Asteman, M. Spiegel, A. Savan, and A. Ludwig, *Applied Surface Science*, **255**, 1850 (2008).
42. Z. Yang, G. Xia, Z. Nie, J. Templeton, and J. W. Stevenson, *Electrochemical and Solid-State Letters*, **11**, B140 (2008).
43. P. Wei, X. Deng, M. R. Bateni, and A. Petric, *Corrosion*, **63**, 529 (2007).
44. A. Petric and H. Ling, *Journal of the American Ceramic Society*, **90**, 1515 (2007).
45. Z. H. Bi, J. H. Zhu, and J. L. Batey, *Journal of Power Sources*, **195**, 3605 (2010).
46. B. Hua, W. Zhang, J. Wu, J. Pu, B. Chi, and L. Jian, *Journal of Power Sources*, **195**, 7375 (2010).
47. G. Jalilvand and M.-A. Faghihi-Sani, *International Journal of Hydrogen Energy*, **38**, 12007 (2013).
48. Z. Lu, G. Xia, J. D. Templeton, X. Li, Z. Nie, Z. Yang, and J. W. Stevenson, *Electrochemistry Communications*, **13**, 642 (2011).
49. W. Huang, S. Gopalan, U. B. Pal, and S. N. Basu, *Journal of The Electrochemical Society*, **155**, B1161 (2008).
50. Z. Yang, G. Xia, and J. W. Stevenson, *Electrochemical and Solid-State Letters*, **8**, A168 (2005).
51. Z. Yang, G.-G. Xia, X.-H. Li, and J. W. Stevenson, *International Journal of Hydrogen Energy*, **32**, 3648 (2007).
52. B. Hua, J. Pu, W. Gong, J. Zhang, F. Lu, and L. Jian, *Journal of Power Sources*, **185**, 419 (2008).
53. J. Wu, Y. Jiang, C. Johnson, and X. Liu, *Journal of Power Sources*, **177**, 376 (2008).
54. J. P. Choi, K. Scott Weil, Y. Matt Chou, J. W. Stevenson, and Z. Gary Yang, *International Journal of Hydrogen Energy*, **36**, 4549 (2011).
55. H. Zhang, J. Wu, X. Liu, and A. Baker, *International Journal of Hydrogen Energy*, **38**, 5075 (2013).
56. T. Uehara, N. Yasuda, M. Okamoto, and Y. Baba, *Journal of Power Sources*, **196**, 7251 (2011).
57. A. Kruk, M. Stygar, and T. Brylewski, *J Solid State Electrochem*, **17**, 993 (2013).
58. J.-H. Kim, R.-H. Song, and S.-H. Hyun, *Solid State Ionics*, **174**, 185 (2004).
59. B.-K. Park, J.-W. Lee, S.-B. Lee, T.-H. Lim, S.-J. Park, C.-O. Park, and R.-H. Song, *International Journal of Hydrogen Energy*, **38**, 12043 (2013).
60. D. R. Ou, M. Cheng, and X.-L. Wang, *Journal of Power Sources*, **236**, 200 (2013).
61. J. Wu, C. D. Johnson, Y. Jiang, R. S. Gemmen, and X. Liu, *Electrochimica Acta*, **54**, 793 (2008).
62. W. Wei, W. Chen, and D. G. Ivey, *Journal of Power Sources*, **186**, 428 (2009).
63. M. J. Lewis and J. H. Zhu, *Electrochemical and Solid-State Letters*, **14**, B9 (2011).
64. W. J. Quadackers, H. Greiner, M. Hänsel, A. Pattanaik, A. S. Khanna, and W. Malléner, *Solid State Ionics*, **91**, 55 (1996).
65. J. Puranen, J. Lagerbom, L. Hyvärinen, M. Kylmälahti, O. Himanen, M. Pihlatie, J. Kiviahio, and P. Vuoristo, *J Therm Spray Tech*, **20**, 154 (2011).
66. O. Thomann, M. Pihlatie, M. Rautanen, O. Himanen, J. Lagerbom, M. Mäkinen, T. Varis, T. Suhonen, and J. Kiviahio, *J Therm Spray Tech*, **22**, 631 (2013).
67. H. Zhang, Z. Zhan, and X. Liu, *Journal of Power Sources*, **196**, 8041 (2011).
68. V. I. Gorokhovskiy, P. E. Gannon, M. C. Deibert, R. J. Smith, A. Kayani, M. Kocpczyk, D. VanVorous, Z. Yang, J. W. Stevenson, S. Visco, C. Jacobson, H. Kurokawa, and S. W. Sofie, *Journal of The Electrochemical Society*, **153**, A1886 (2006).
69. C. C. Mardare, M. Spiegel, A. Savan, and A. Ludwig, *Journal of The Electrochemical Society*, **156**, B1431 (2009).
70. J.-J. Choi, J. Ryu, B.-D. Hahn, W.-H. Yoon, B.-K. Lee, and D.-S. Park, *J Mater Sci*, **44**, 843 (2009).
71. W. Zhang, B. Hua, N. Duan, J. Pu, B. Chi, and J. Li, *Journal of The Electrochemical Society*, **159**, C388 (2012).
72. H. Ebrahimifar and M. Zandrahimi, *Oxid Met*, **75**, 125 (2011).
73. H. Ebrahimifar and M. Zandrahimi, *Ionics*, **18**, 615 (2012).
74. Z. A. Munir, U. Anselmi-Tamburini, and M. Ohyanagi, *J Mater Sci*, **41**, 763 (2006).
75. A. L. G. Prette, M. Cologna, V. Sglavo, and R. Raj, *Journal of Power Sources*, **196**, 2061 (2011).
76. S. Naka, M. Inagaki, and T. Tanaka, *J Mater Sci*, **7**, 441 (1972).
77. Z. Yang, G. Xia, S. P. Simmer, and J. W. Stevenson, *Journal of The Electrochemical Society*, **152**, A1896 (2005).
78. D. G. Wickham and W. J. Croft, *Journal of Physics and Chemistry of Solids*, **7**, 351 (1958).
79. E. Aukrust and A. Muan, *Journal of the American Ceramic Society*, **46**, 511 (1963).
80. L. A. Chick, L. R. Pederson, G. D. Maupin, J. L. Bates, L. E. Thomas, and G. J. Exarhos, *Materials Letters*, **10**, 6 (1990).
81. M. Mariñšek, K. Zupan, and J. Maček, *Journal of Materials Research*, **18**, 1551 (2003).
82. A. V. Ragulya and V. V. Skorokhod, *Nanostructured Materials*, **5**, 835 (1995).
83. J. R. Groza and R. J. Dowding, *Nanostructured Materials*, **7**, 749 (1996).
84. J. R. Groza, *Nanostructured Materials*, **12**, 987 (1999).
85. B. B. Panigrahi, M. M. Godkhindii, K. Das, P. G. Mukunda, V. V. Dabhade, and P. Ramakrishnan, *Journal of Materials Research*, **20**, 827 (2005).
86. W. Qu, L. Jian, J. M. Hill, and D. G. Ivey, *Journal of Power Sources*, **153**, 114 (2006).
87. X. Xin, S. Wang, Q. Zhu, Y. Xu, and T. Wen, *Electrochemistry Communications*, **12**, 40 (2010).
88. S. Fontana, S. Chevalier, and G. Caboche, *Materials and Corrosion*, **62**, 650 (2011).
89. Y. Zhang, A. Javed, M. Zhou, S. Liang, and P. Xiao, *International Journal of Applied Ceramic Technology*, **11**, 332 (2014).
90. B. Hua, J. Pu, F. Lu, J. Zhang, B. Chi, and L. Jian, *Journal of Power Sources*, **195**, 2782 (2010).
91. Y.-S. Chou, J. W. Stevenson, and J.-P. Choi, *Journal of Power Sources*, **255**, 1 (2014).
92. L. Blum, U. Packbier, I. C. Vinke, and L. G. J. de Haart, *Fuel Cells*, **13**, 646 (2013).
93. Z. Yang, J. S. Hardy, M. S. Walker, G. Xia, S. P. Simmer, and J. W. Stevenson, *Journal of The Electrochemical Society*, **151**, A1825 (2004).
94. N. Shaigan, D. G. Ivey, and W. Chen, *Journal of Power Sources*, **183**, 651 (2008).
95. H. Ebrahimifar and M. Zandrahimi, *Surface and Coatings Technology*, **206**, 75 (2011).
96. R. Trebbels, T. Markus, and L. Singheiser, *Journal of Fuel Cell Science and Technology*, **7**, 011013 (2009).
97. W. N. Liu, X. Sun, E. Stephens, and M. A. Khaleel, *Journal of Power Sources*, **189**, 1044 (2009).
98. S. Taniguchi, M. Kadowaki, H. Kawamura, T. Yasuo, Y. Akiyama, Y. Miyake, and T. Saitoh, *Journal of Power Sources*, **55**, 73 (1995).
99. S. P. S. Badwal, R. Deller, K. Foger, Y. Ramprakash, and J. P. Zhang, *Solid State Ionics*, **99**, 297 (1997).